

**EARLY CHANNEL EVOLUTION IN THE MIDDLE PERMIAN BRUSHY
CANYON FORMATION, WEST TEXAS, USA**

A Thesis

by

SPENCER BLAKE GUNDERSON

Submitted to the Office of Graduate Studies of
Texas A&M University
in partial fulfillment of the requirements for the degree of

MASTER OF SCIENCE

August 2011

Major Subject: Geology

**EARLY CHANNEL EVOLUTION IN THE MIDDLE PERMIAN BRUSHY
CANYON FORMATION, WEST TEXAS, USA**

A Thesis

by

SPENCER BLAKE GUNDERSON

Submitted to the Office of Graduate Studies of
Texas A&M University
in partial fulfillment of the requirements for the degree of

MASTER OF SCIENCE

Approved by:

Chair of Committee,	Michael Tice
Committee Members,	Walter Ayers
	Thomas Olszewski
	Robert Weiss
Head of Department,	Andreas Kronenberg

August 2011

Major Subject: Geology

ABSTRACT

Early Channel Evolution in the Middle Permian Brushy Canyon Formation, West Texas,
USA. (May 2011)

Spencer Blake Gunderson, B.A., The University of California, Berkeley

Chair of Advisory Committee: Dr. Michael Tice

Submarine channels are important conduits for sediment in deep marine environments, and understanding their formation is critical to modeling basin fill processes. Most models describing channel evolution focus on turbidity currents as the erosive and constructive force in channel initiation. However, slope failure and slumping can be significant drivers of channelization, particularly in upper slope and ramp environments. Determining the relative roles of slumping and erosion by turbidity currents can provide important insight into the timing of channelization and the geometries of subsequent deposits. Samples were collected from Guadalupe Mountains National Park from two primary localities at Salt Flat Bench (Figure 2). Three vertical sections were measured at both locations. A total of 16 samples were collected for petrographic analysis and X-ray fluorescence (XRF) imaging.

Spectacular outcrop quality makes the Middle Permian Brushy Canyon Formation in Guadalupe Mountains National Park an ideal location for the study of early channel evolution. A detailed facies analysis of fine-grained channel deposits was conducted in the Upper Brushy Canyon Formation in the Salt Flat Bench outcrops. After channelization, an interval of relative condensation dominated by hemipelagic settling of organic matter and silt was followed by an interval of incomplete sediment bypass by turbidity currents. This sequence of events suggests that sea level was at a relative highstand at the time of channel inception, whereas channel inception by turbidity

currents is expected during a lowstand. Slumping rather than erosion by turbidity currents is the most likely mechanism to have initiated a channel at the study area. There is no evidence for the existence for high energy currents until after the interval of condensation. However, the action of weak contour currents during early channel evolution is observed in outcrop and microtextural features. Early carbonate cementation of channel-lining silts may have stabilized the slump surface with respect to erosion by later turbidity currents.

ACKNOWLEDGEMENTS

Thanks first and foremost to my adviser, Dr. Michael Tice. His assistance and immense knowledge have been invaluable. My study of the Brushy Canyon Formation started during a course taken in the fall of 2009. Thanks to my adviser and Dr. Thomas Olszewski for their leadership in this course on geobiological field methods. This sparked my interest in the Brushy Canyon Formation. To the other members of my committee, Dr. Robert Weiss and Dr. Walter Ayers, your insights have been most appreciated. Thanks to Kannipa Motanated for her help in the field and to the National Parks Department for their cooperation.

TABLE OF CONTENTS

	Page
ABSTRACT	iii
ACKNOWLEDGEMENTS	v
TABLE OF CONTENTS	vi
LIST OF FIGURES	vii
1. INTRODUCTION.....	1
2. GEOLOGIC SETTING.....	4
3. METHODS.....	7
3.1 XRF Scanning Methods	7
3.2 Grain Size and Textural Analysis.....	7
4. RESULTS.....	8
4.1 Five Facies.....	9
5. DISCUSSION	20
5.1 Current Activity during Siltstone Deposition.....	20
5.2 Siltstone Diagenesis	21
5.3 Model for Channel Evolution.....	22
6. CONCLUSIONS.....	25
REFERENCES	27
APPENDIX	32
VITA	35

LIST OF FIGURES

	Page
Figure 1: Models of submarine channels	3
Figure 2: Permian basin, stratigraphic column and study area	5
Figure 3: Facies description	8
Figure 4: Coarse-grained lag deposit	10
Figure 5: Facies distributions on northwest Salt Flat Bench	11
Figure 6: Grain size and terminal fall velocity	14
Figure 7: Heavy and light mineral grain orientations	17
Figure 8: Model fit of grain orientation distribution to Von Mises distribution.....	18
Figure 9: Diagenetic features	19
Figure 10: Model for channel initiation and early evolution at Salt Flat Bench	24

1. INTRODUCTION

Spectacular outcrop exposures have made the Brushy Canyon Formation (BCF) a model system for studying channel filling processes (Beaubouef et al., 1999; Fischer and Sarnthein, 1988; Gardner, 2003; Gardner and Borer, 2000; Gardner et al., 2010; Hardage et al., 1998; King, 1948; Pyles et al., 2010; Ye and Kerans, 1996); however, the processes initiating flow confinement on an unchannelized bed are relatively less studied in this unit. It is generally accepted that unconfined turbidity currents are capable of initiating channels by erosion, the deposition of levees, or a combination of the two (Figure 1) (Beaubouef et al., 1999; Fedele and García, 2009; Imran et al., 2002; Rowland et al., 2010). Clear levee deposits are absent in the Brushy Canyon Formation (Beaubouef et al., 1999; Harms and Brady, 1996), probably reflecting a lack of sediment cohesiveness resulting from a paucity of clay transported into the basin (Fischer and Sarnthein, 1988; Harms and Brady, 1996). This suggests that levee construction was not a significant factor in channelization on the BCF ramp.

Other investigators have proposed channel evolution models in which erosive processes initiated channel development. Harms and Brady (1996) hypothesized that sediment-poor hypersaline or cold density currents eroded silty ramp sediments to form channels. Later tractional transport and deposition from density currents produced distinctive channel-lining siltstones prior to being filled with coarser sediments. In contrast, Beaubouef et al. (1999) suggested that channels were incised by a combination of erosive turbidity currents and slumping. In this model, channel-lining siltstones were deposited from the tails of otherwise bypassing turbidity currents as the erosive power of average currents decreased. Gardner and Borer (2000) proposed the “build-cut-fill-spill” model, in which flows were focused through topographic lows between deposits of unconfined turbidity currents. Initial flow confinement led to downcutting and further channelization. Overall channel location and migration in the

This thesis follows the style of *Sedimentary Geology*.

upper ramp was controlled by pre-existing topography formed by slumping. In this model, channel-lining siltstones were deposited by bypassing turbidity currents or by hemipelagic sedimentation during intervals of relative condensation (Beaubouef et al., 1999; Pyles et al., 2010; Sageman et al., 1998).

Determining the relative roles of slumping and erosion by turbidity currents in channel initiation is important for understanding the timing of channel formation with respect to sea level cycles, the distribution of resulting sediment routing networks, and the geometries of submarine channel deposits. In the BCF, channel-lining siltstones provide a record of environmental conditions and sedimentary processes following channel formation. Interpretation of these rocks is therefore critical to inferring channelization processes as well as evaluating existing models of channel evolution. Hemipelagic siltstones deposited following slumping will be distributed within channels and the surrounding seafloor. They may show evidence of slow accumulation and long intervals of exposure to seawater in the form of intense diagenetic alteration, reworking by weak currents and elevated organic content (Johnson-Ibach, 1982). In contrast, siltstones deposited by bypassing turbidity currents may be confined to paleotopographic lows and preserve evidence of stronger currents or the passage of coarser material (e.g. lag deposits).

In order to determine the relative timing of slumping and the flow of turbidity currents during early channel evolution, we conducted a detailed facies characterization of channel-lining siltstones within the Upper BCF. Field observations, x-ray fluorescence microscopy and petrography of the channel-lining siltstones allowed the identification of facies distributions and microtextures indicative of different depositional and diagenetic processes. The inferred depositional and diagenetic histories of these siltstones were used to determine whether turbidity currents were flowing at or around the same time as slumping during early channel evolution recorded in the Salt Flat Bench.

A. Erosional



B. Mixed



C. Depositional

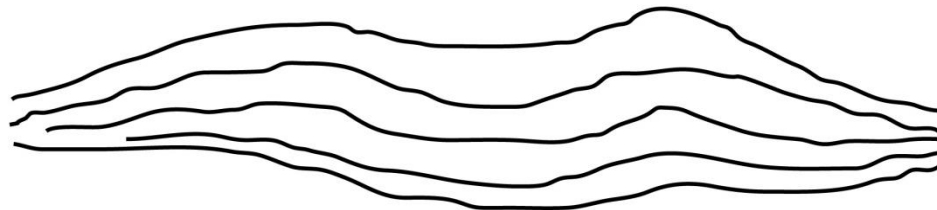


Figure 1: Models of submarine channels. Submarine channels are commonly formed by the passage of turbidity currents. A) Erosional channels are formed by localized scouring by turbidity currents followed by flow focusing and downcutting. B) Mixed-type channels are formed by a combination of downcutting and levee construction. C) Depositional channels are formed primarily by construction of cohesive levees. Modified from Imran (2002).

2. GEOLOGIC SETTING

The Permian Basin complex was initiated during Mississippian to Early Pennsylvanian time. Crustal shortening from the Marathon fold-and-thrust belt resulted in a foreland basin to the north. Isostatic rebound followed in the Early Permian (Wolfcampian) resulting in an angular unconformity extending across the basin margin (Beaubouef et al., 1999; Sageman et al., 1998). Following the mid-Wolfcampian unconformity, subsidence rates decreased from 3.7 cm/kyrs to .8 cm/ky by the end of Guadalupian (Ye and Kerans, 1996). Permian strata within Guadalupe Mountains National Park were deposited in the Delaware Basin, a sub-basin of the Permian Basin complex (Figure 2). The Delaware Basin was covered by an epicontinental sea and connected to the Panthalassa Ocean by only a narrow channel (Pyles et al., 2010). At the time the Brushy Canyon Formation was deposited, water depths are estimated to have been 400 to 600 m (Beaubouef et al., 1999).

The Brushy Canyon Formation unconformably overlies the Guadalupian Cutoff Formation and Pipeline Shale (Pyles et al., 2010). The Upper Cutoff is composed of thinly bedded dark limestones. The Pipeline Shale is the more distal equivalent of the Upper Cutoff Formation and is composed of organic rich siltstones (Sageman et al., 1998). The Brushy Canyon Formation is composed of up to 460 m of sandstones and siltstones representing canyon fill, slope deposits, and basin floor deposits onlapping the underlying carbonate slope (Gardner and Borer, 2000). Stacked channels form channel complexes up to 1 km in width and 40 m deep.

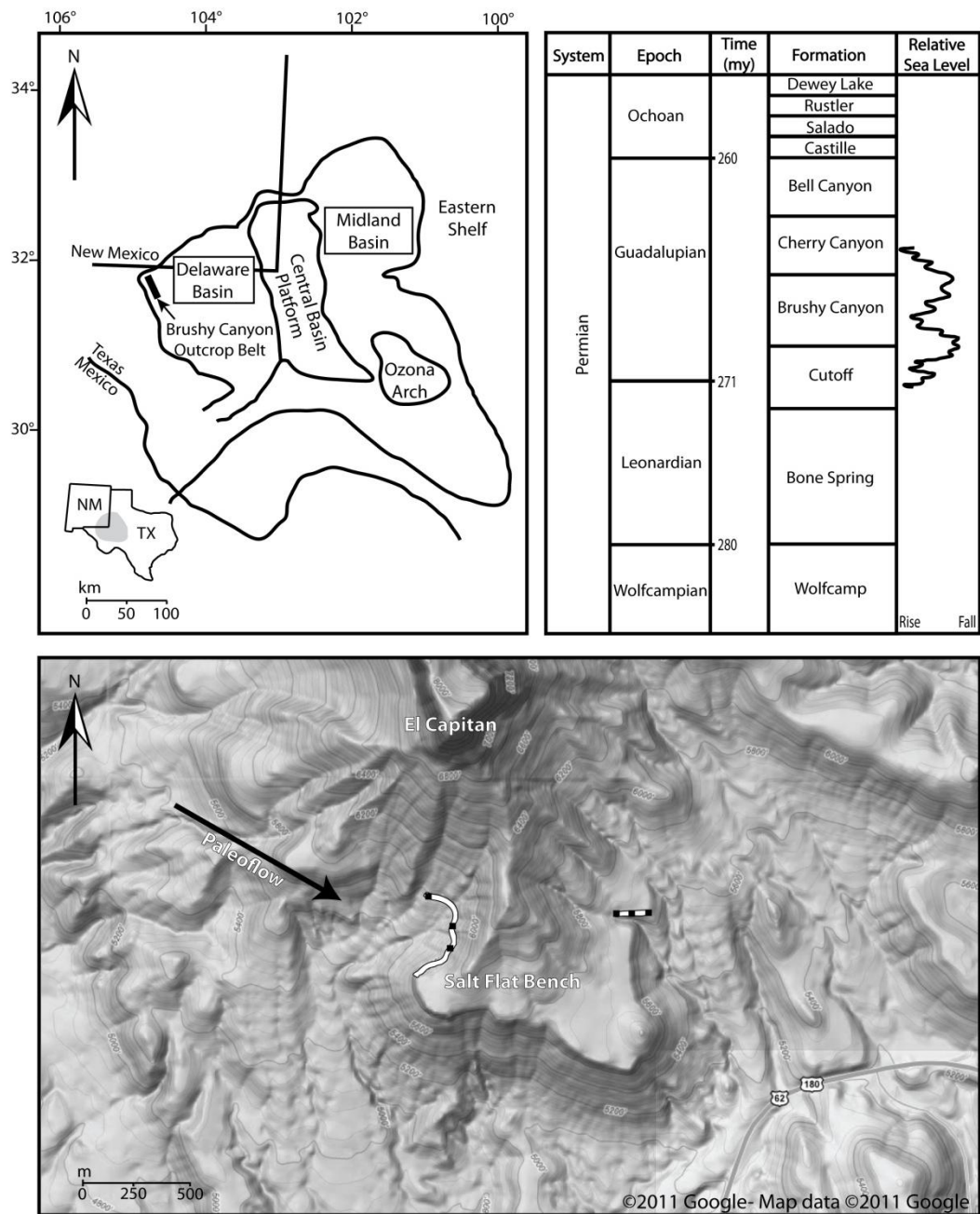


Figure 2: Permian basin, stratigraphic column and study area. Paleogeography of the Permian Basin complex modified from (Beaubouef et al., 1999; Dutton et al., 2003); stratigraphic column for the Delaware basin with relative sea level curve modified from (Dutton et al., 2003; Sageman et al., 1998); Shaded elevation map showing area of study south of El Capitan and location of vertical sections (black squares), modified from (Google, 2011). Paleoflow direction is 120° (Gardner and Borer, 2000).

Paleoflow indicators show that outcrops in the area of study were sourced from the northwest (Gardner and Borer, 2000; Pyles et al., 2010). An unconformity on the shelf correlates with Brushy Canyon Strata and suggests that the shelf was exposed during a sea level lowstand (Pyles et al., 2010). The Brushy Canyon Formation is a third order lowstand system tract sequence set, deposited over approximately 2 million years (Gardner and Borer, 2000). It has been further divided into three fourth order cycles: the Lower, Middle and Upper Brushy Canyon, and nine fifth order cycles (Gardner and Borer, 2000).

Salt Flat Bench provides cross sectional views of a submarine fan complex confined to a kilometer-scale slump-scar depression (Gardner and Borer, 2000; Sageman et al., 1998). The architecture of channel-filling facies has been described in detail by Gardner and Borer (2000). The topography of the modern erosion surface provides a unique three-dimensional exposure of the channel and access to channel-lining siltstones from margin to axis.

3. METHODS

Samples were collected from Guadalupe Mountains National Park from two primary localities at Salt Flat Bench (Figure 2). Three vertical sections were measured at both locations. A total of 16 samples were collected for petrographic analysis and x-ray fluorescence (XRF) imaging.

3.1 XRF Scanning Methods

Cut slabs were scanned using a Horiba XGT-7000 X-ray Analytical Microscope in order to map spatial distributions of elements. Scans were conducted over 25.6 x 25.6 mm squares at 100 μm resolution to characterize laminations, concretions and other relatively large features. 10 μm resolution scans over 5.12 x 5.12 mm squares were then conducted on identified features of interest to measure the diameters and orientations of individual grains. All scans were conducted with an accelerating voltage of 50 kV and a 1 mA current applied to a rhodium source. Full spectra were conducted from 0-40 keV, and elemental distribution maps were generated by integrating around background-corrected K_{α} fluorescence lines of K, Zr, Ti, Ba and S.

3.2 Grain Size and Textural Analysis

Major and minor axes of mineral grains were measured optically in thin section and using 10 μm maps of associated elemental fluorescence lines. The full width at half the maximum intensity, measured across grain transects, was used to estimate grain diameters. Element maps and photomicrographs were overlaid by digital grids with spacing at least twice that of the largest grain diameter. The single grain with its center closest to each node was measured. Geometric means of long and short axes were used to estimate grain size. Grain inclinations with respect to the horizontal were also measured on vertical faces cut both parallel and perpendicular to paleoflow indicators in overlying sandstones. Orientations were expressed as inclinations from -90° to 90° and plotted on Rose diagrams for comparison.

4. RESULTS

Five facies were identified in outcrops at Salt Flat Bench: 1) the gray siltstone facies; 2) the black siltstone facies; 3) the brown siltstone facies; 4) the thinly bedded sandstone facies and; 5) the structureless sandstone facies (Fig. 3).

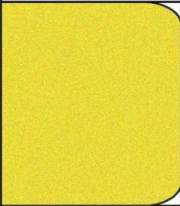

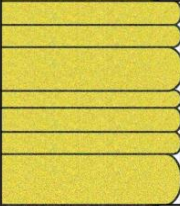


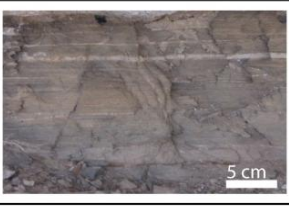

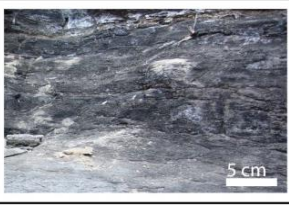


Vertical Sections Legend	Outcrop Photograph	Facies Name and Interpretation
		<u>Structureless Sandstone:</u> Bouma A and D divisions deposited by high-density turbidity currents
		<u>Thinly Bedded Sandstone:</u> Bouma C and D divisions deposited by turbidity currents
		<u>Brown Siltstone:</u> Deposited from channel confined turbidity currents which primarily bypassed the study site (Incomplete bypass)
		<u>Black Siltstone:</u> Deposited by pelagic and hemipelagic settling
		<u>Gray Siltstone:</u> Siltstones deposited by pelagic and hemipelagic settling with interbedded sandstone deposited by unconfined turbidites

Figure 3: Facies description. Vertical sections legend showing outcrop photographs, facies names and interpretations.

4.1 Five Facies

Gray Siltstone. The gray siltstone facies is composed of finely and evenly laminated sandy siltstone with rare thin (<3 cm thick) interbeds of laterally continuous very fine sandstone. Sand beds are plane or cross laminated. This facies comprises >90% of the Brushy Canyon Formation and, in the study location, forms the unit into which the channel was incised. It has been interpreted as deposits from unconfined turbidity currents (Beaubouef et al., 1999) or as pelagic deposits transported to the basin by wind (Fischer and Sarnthein, 1988).

Black Siltstone. The black siltstone facies is composed of finely and evenly laminated carbonaceous siltstone. These siltstones form laterally continuous marker horizons in the Brushy Canyon Formation, and are interpreted as relatively condensed deposits of hemipelagic settling (Beaubouef et al., 1999; Fischer and Sarnthein, 1988; Gardner and Borer, 2000; Sageman et al., 1998). In the study area, the black siltstone facies forms a drape on the basal master surface, and is thickest on the northwest channel margin. This facies weathers to a light-grey or tan color, making it difficult to distinguish from the gray siltstone in certain instances. However, scraping away the weathered surface or tracing beds laterally typically resolves ambiguous interpretations.

Brown Siltstone. The brown siltstone facies is composed of dark brown siltstone with discontinuous fine sandstone stringers and rare sandstone cobbles. Siltstones are finely but discontinuously laminated, and sandstone stringers are typically cross laminated. Where present, sandstone clasts lie on the updip (northwest) sides of sandstone stringers (Fig. 4), suggesting that sand was deposited as downflow lags behind small obstructions. This is a previously undocumented sedimentary structure that clearly illustrates the bypass of large volumes of sediment. The consistent location of lag deposits on one side of oversized clasts provides an additional paleoflow direction indicator. The brown siltstone is present only near the channel axis, and always overlying thin black siltstone. This facies is interpreted as having been deposited by channel-confined turbidity

currents which primarily bypassed the study location. It weathers recessively relative to the underlying black siltstone and overlying sandstone beds.



Figure 4: Coarse-grained lag deposit. Outcrop photograph of the brown siltstone facies with flow from left to right. Sand grains transported as bedload are forced to slow and are deposited basinward of the obstacle.

Thinly Bedded Sandstone. The thinly bedded sandstone facies is composed of 1–10-cm-thick laminated and cross laminated beds of very fine sandstone. This facies is thickest along the northwest channel margin and grades laterally into the channel into structureless sandstones. Beds are frequently bimodal in carbonaceous content, occasionally giving the appearance of interbedded sandstone and black siltstone. However, laterally equivalent structureless sandstones also alternate between light, relatively clean beds and dark, carbonaceous beds, suggesting deposition by the same mechanisms. This facies is interpreted as stacked Bouma C and D divisions deposited by low density turbidity currents.

Structureless Sandstone. The structureless sandstone facies is composed of 10–50-cm-thick beds of massive to normally graded fine to very fine sandstone capped by 2–10-mm-thick layers of laminated siltstone. Cross laminated intervals are rare and most commonly observed on bedding planes. Sandstones are bimodal in carbonaceous content and can appear as alternating dark gray and light gray beds. They frequently contain floating siltstone intraclasts. This facies is thickest along the channel axis. It is

interpreted as the deposits of high density turbidity currents dominated by Bouma A and D divisions.

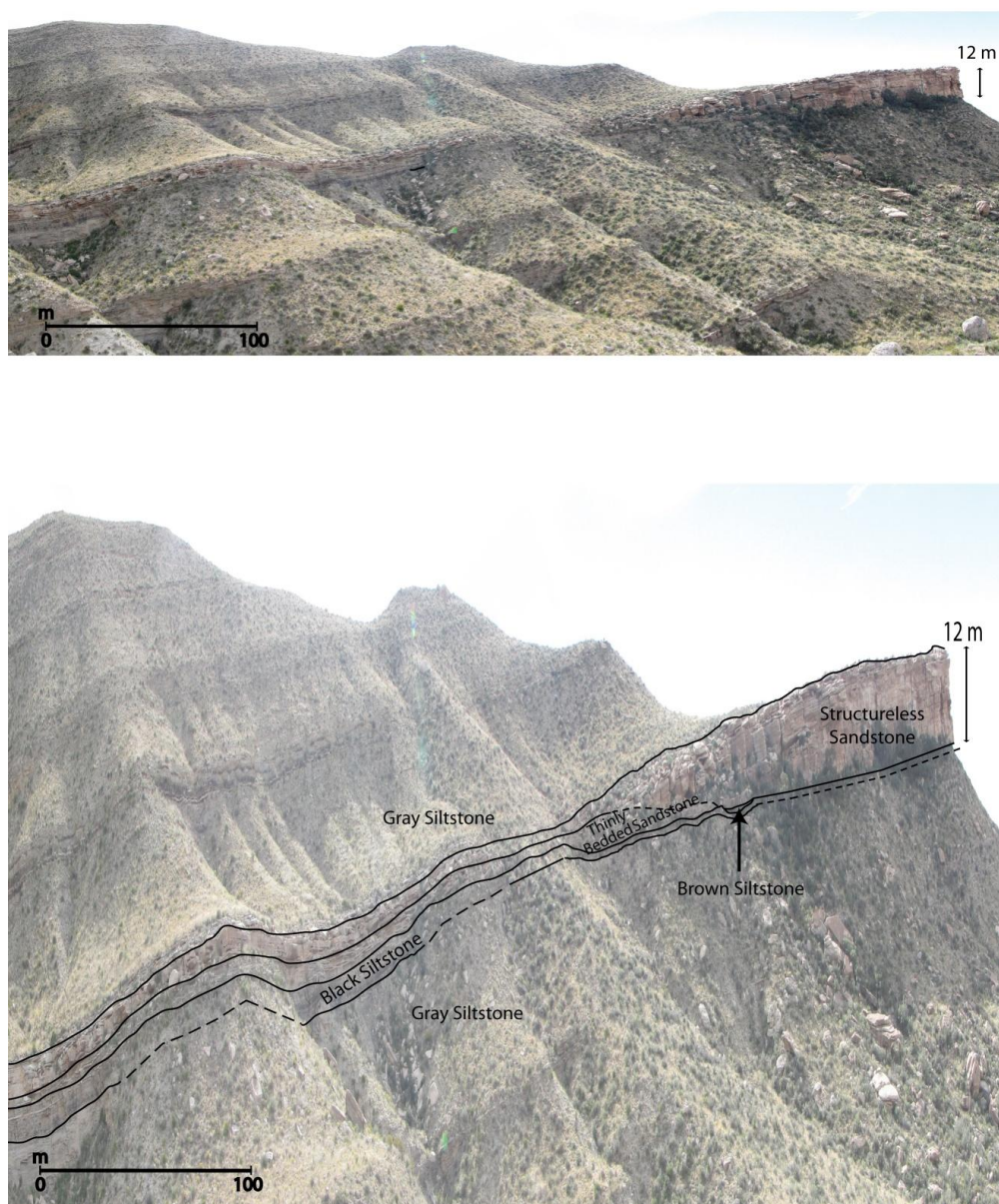


Figure 5: Facies distributions on northwest Salt Flat Bench. A) Panoramic photograph in true scale and B) in 3X vertical exaggeration with facies locations and relationships illustrated. The black siltstone facies drapes the master surface and thickens toward the channel margin. The brown siltstone is present only in a small lens located near the thickest part of the channel.

The outcrop studied on the western side of Salt Flat Bench is U-shaped, providing both dip and strike-oriented perspectives (Fig. 5). The strike-oriented face of the outcrop is dominated by 12 m of thick structureless sand beds. These thin dramatically toward the northwest and become more thinly bedded. The sand beds onlap the underlying black siltstone and thinly bedded sandstone at the northernmost portion of the strike section. The black siltstone is thickest (270 cm) at its furthest point from the channel axis. The black siltstone drapes underlying topography. The brown siltstone facies is mostly absent in this outcrop, with the exception of a <10-m-wide lenticular bed.

An outcrop on the eastern side of Salt Flat Bench is oriented nearly parallel to flow and provides a dip-elongate perspective. The structureless and thin bedded sandstone again form prominent cliffs. The channel filling sandstone beds here are 4 m thick in the middle of the outcrop. The black siltstone facies is laterally continuous and lines the base of the channel form. A brown siltstone layer overlies the basal black siltstone and is continuous along the 200 m length of the outcrop at a nearly constant thickness of 10–12 cm.

Size distributions of zircon and rutile grains were estimated for the black and brown siltstone facies (X samples) by XRF imaging of Zr and Ti, respectively, and distributions for quartz and feldspar grains were estimated by optical petrography (seven samples). The brown and black siltstones have statistically indistinguishable quartz and feldspar grain size distributions ($P = 0.39$ on a t-test for means and $P = 0.14$ on an F-test for variances), with a mean grain size of 4.21ϕ ($54 \mu\text{m}$) and a standard deviation of 1.0ϕ . Normal probability plots (Filliben, 2010) of grain size were constructed (Fig. 6) by plotting sorted grain sizes against corresponding normal statistic medians (Eq. 1).

$$n_i = \text{erf}^{-1}(2u_i - 1), \quad (1)$$

where

$$u_i = \begin{cases} 1 - 0.5^{1/N} & \text{for } i = 1 \\ \frac{i - .3175}{N + .365} & \text{for } i > 1 \end{cases}, \quad (2)$$

N is the number of measurements, and i is the rank of the given measurement. Normally distributed data plot as straight lines under this transformation.

Terminal fall velocities were calculating using equation 3 to examine sorting mechanisms (Julien, 1998).

$$\omega = \frac{8v_m}{d} \left[(1 + .0139d_*^3)^{0.5} - 1 \right], \quad (3)$$

where ω is the terminal settling velocity, d is the grain diameter, v_m is the kinematic viscosity, G is the specific gravity, g is the acceleration due to gravity and d_* is the dimensionless particle diameter:

$$d_* = d \left[\frac{(G-1)g}{v_m^2} \right]^{1/3}. \quad (3)$$

Fall velocity distributions were also examined in normal probability plots. In order to estimate confidence intervals on velocity distributions, a Monte Carlo simulation was performed. 100 simulated velocity distributions were produced for each grain population assuming log-normally distributed relative errors with mean $\ln(1)$ and standard deviation $\ln(1.1)$. Each simulated dataset was sorted as if to produce a normal probability plot. Confidence interval limits were set to be the 16th and 84th percentile velocities for each rank (Fig. 6).

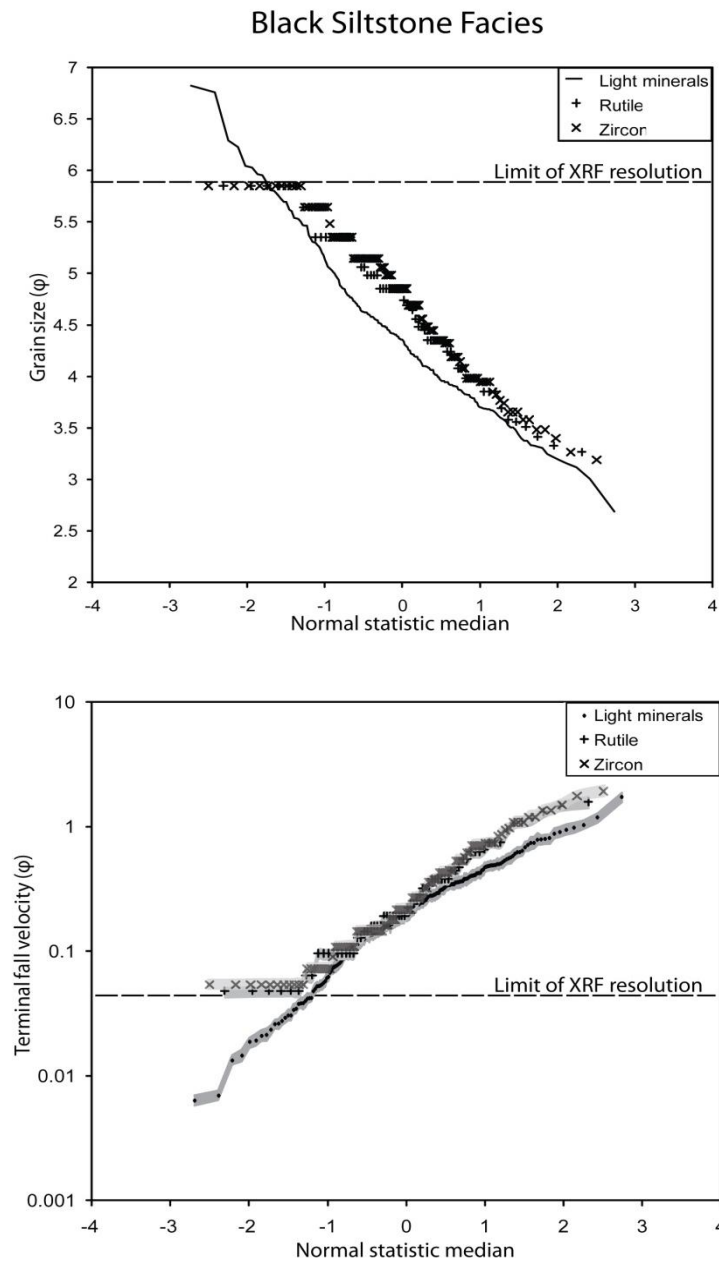


Figure 6: Grain size and terminal fall velocity distributions for the black and brown siltstone facies. Grain size for heavy mineral grains is normally distributed when viewed in the phi scale. Light minerals, zircons, and rutile grains are plotted. XRF grain size measurements cannot resolve grain sizes $>6 \phi$. Confidence intervals on calculated fall velocities are denoted by gray bands.

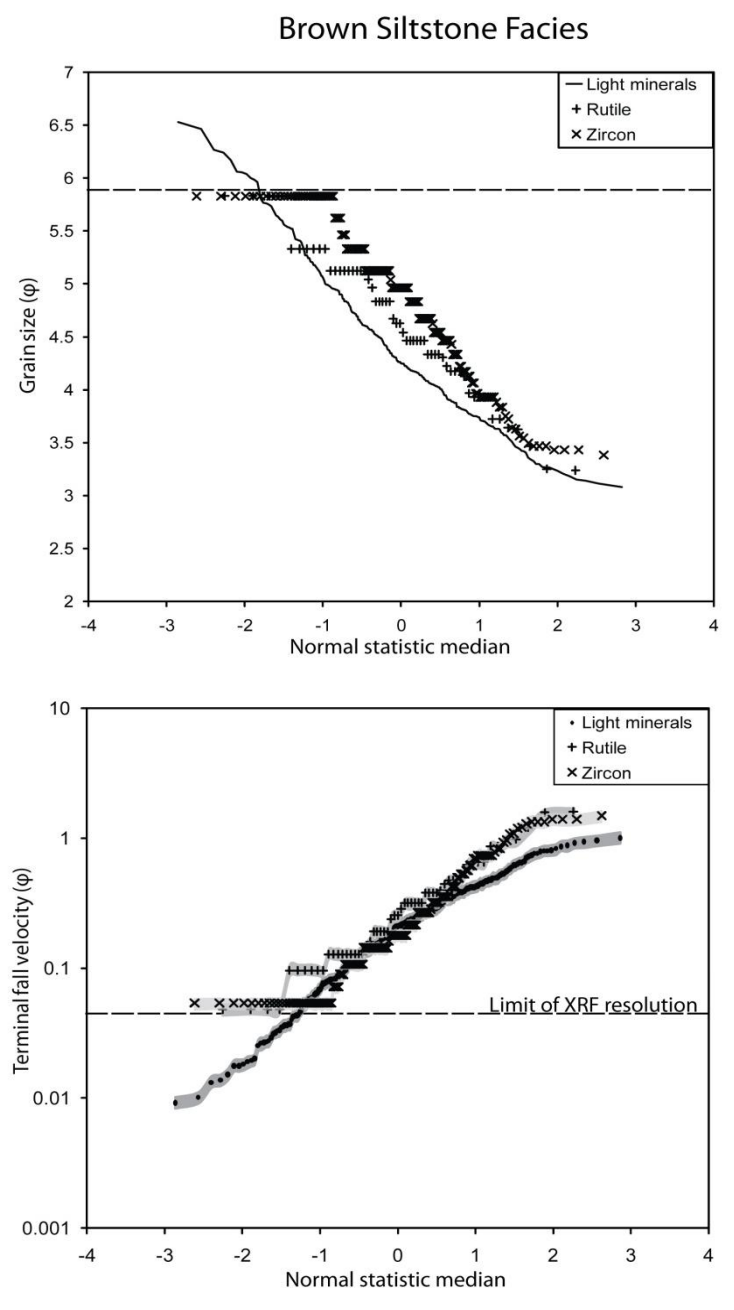


Figure 6: Continued

The inclinations of 906 light mineral grains and 729 heavy mineral grains were measured on surfaces cut parallel to overlying flow indicators. Grain orientation appears bimodal in many of the samples measured both in thin section and XRF, even within individual laminae (Figure 7). To test this observation, orientation data were aggregated and fit by nonlinear least-squares regression with sums of one, two, or three modified von Mises distributions (Eq. 5):

$$f(\theta_i) = \sum_{j=1}^3 a_j \frac{e^{\kappa_j \cos 2(\theta_i - \mu_j)}}{2\pi I_0(\kappa_j)}, \quad (5)$$

where $a_1 + a_2 + a_3 = 1$, κ_j are measures of the concentrations of the distribution about each mode, μ_j are the modes, and $I_0(x)$ is the modified Bessel function of order zero. The model fit for quartz and feldspar grains with two von Mises distributions was significantly better than that with one (F-test, $P = 0.002$), but the fit with three distributions was not better than that with two ($P = 0.57$), confirming that the actual distribution was bimodal. The preferred fit had $a_1 = 0.60$, $\kappa_1 = 2.16$, $\mu_1 = 23.8^\circ$, $a_2 = 0.40$, $\kappa_2 = 2.92$, and $\mu_2 = -32.8^\circ$.

Zircon and rutile grains in slabs cut parallel to paleoflow exhibit a similar distribution and are clustered around the same modes of -20° to -30° and 20° to 30° . The distributions fit two Von Mises distributions less well than the light minerals do. An F-test shows no significant improvement from fitting two Von Mises distributions compared to a fitting to a single distribution ($P=.396$). The most likely reason for this discrepancy is that heavy mineral orientations are not well-modeled by a small number of von Mises distributions since a large fraction of this population was shielded by light mineral grains. This fraction would have simply settled into the interstitial space between quartz and feldspar grains. It is therefore remarkable that the two modes identified in the light grain population are identifiable as distinct peaks in the heavy grain population. In contrast, heavy mineral grains in slabs cut perpendicular to flow indicators in overlying sandstones exhibited a grain orientation distribution with a local

maximum near only one of the modes identified in the light mineral population (between -10° to -20°).

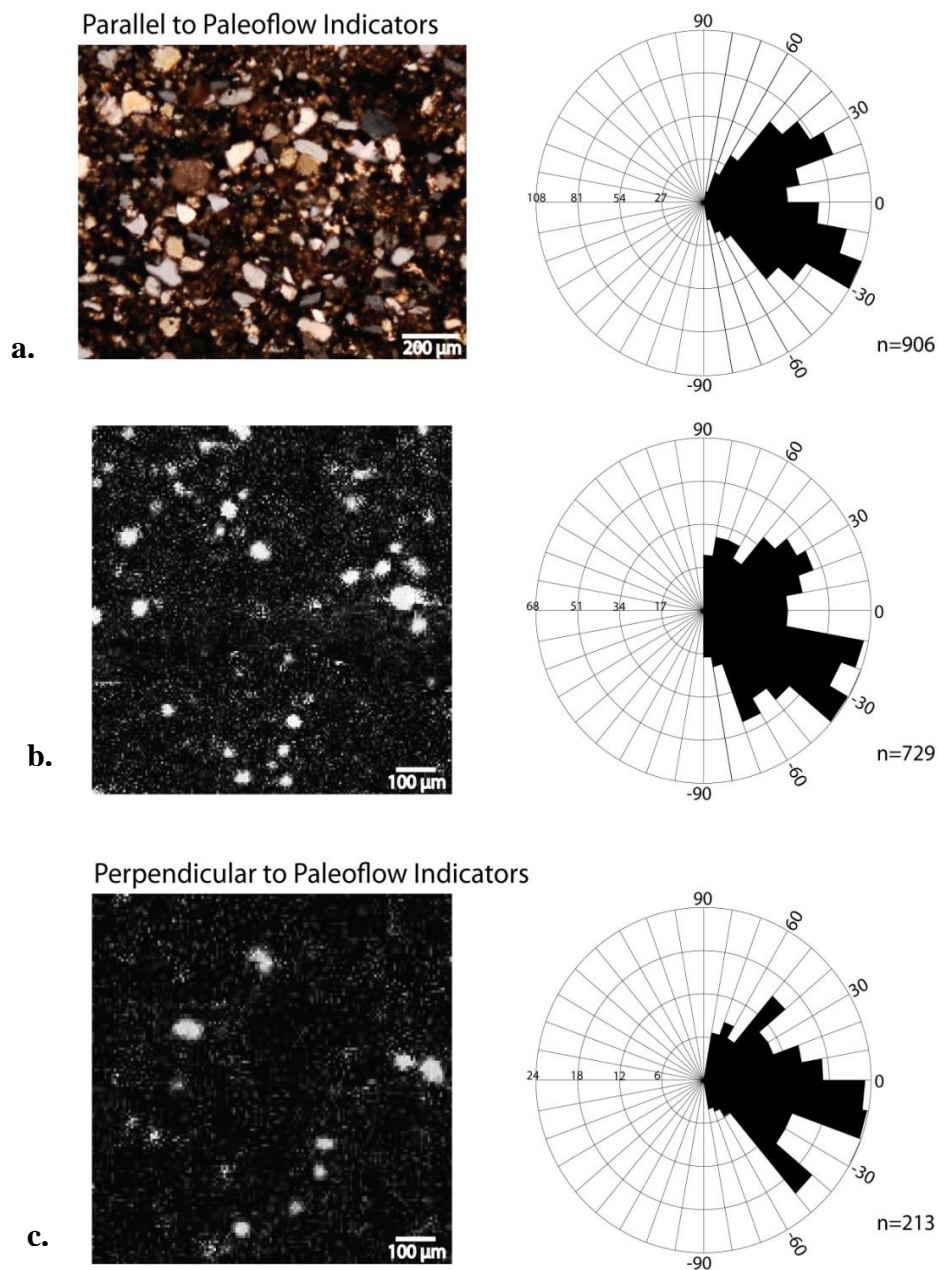


Figure 7: Heavy and light mineral grain orientations. Images of grain orientation and orientation measurements collected optically and by XRF microscopy. a) Both show similar trends from 906 light mineral grains (quartz and feldspar) and 729 heavy mineral grains (rutile and zircon) measured. Grain orientation measurements perpendicular to flow and representative XRF map are shown for comparison. 213 orientation measurements perpendicular to paleoflow were made on heavy minerals.

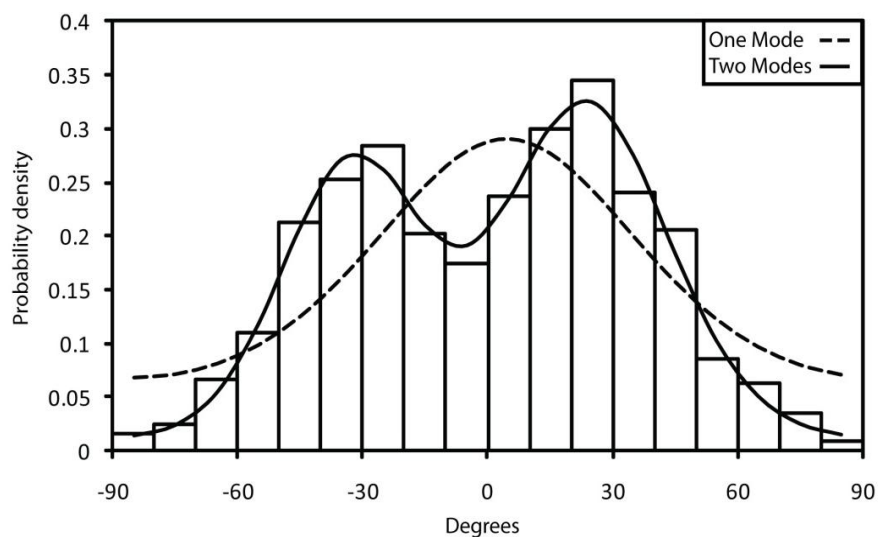


Figure 8: Model fit of grain orientation distribution to Von Mises distribution.

Diagenetic nodules and cements composed of carbonate and sulfate minerals are common in both siltstone facies. Barite concretions in the Brushy Canyon are visible in X-ray fluorescence images as zones of elevated Ba, S, and Sr (Fig. 9). Barite concretions occur as discontinuous laminations and have an average thickness of .6 mm with no examples exceeding 1 mm.

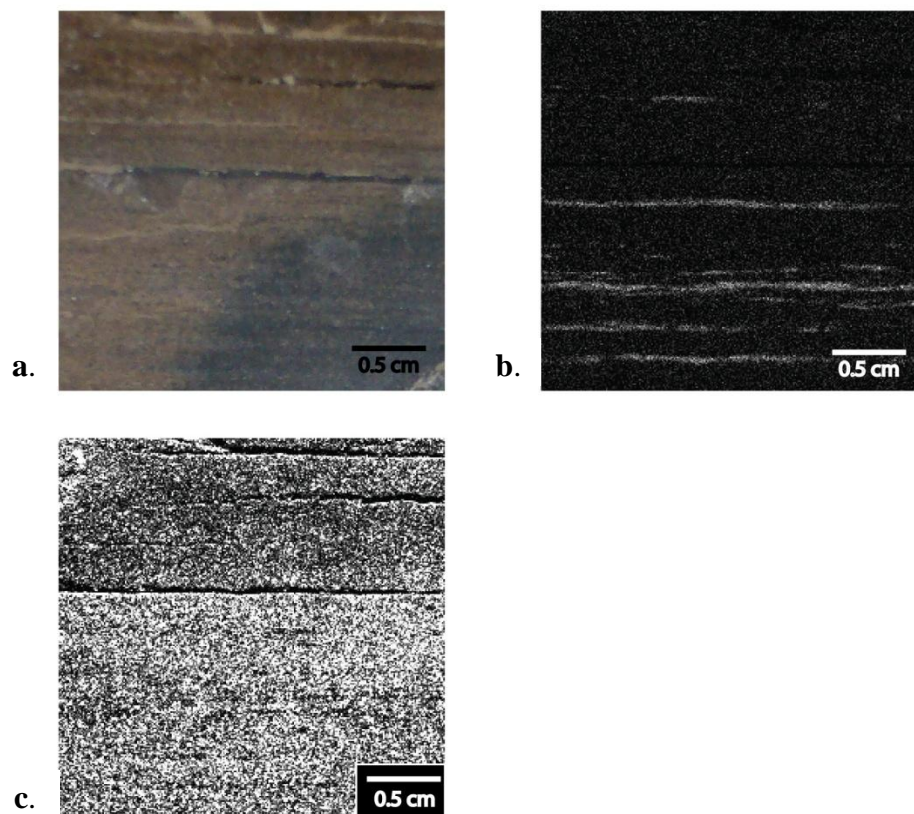


Figure 9: Diagenetic features. a) Photograph of sample GTS3-B showing the contact between the brown and black siltstone facies. b) Barite nodules and laminations just below the contact of the two facies in a 100 μm resolution XRF map of Ba $K_{\alpha 1,2}$ fluorescence intensity. c) A sharp contrast in Ca content imaged in an XRF map of Ca $K_{\alpha 1}$ intensity.

Ca $K_{\alpha 1}$ fluorescence in the brown siltstone is $\sim 60\%$ the intensity of the black siltstone, implying substantially less carbonate cement. This contrast in cementation likely accounts for the sharp difference in susceptibility to weathering observed in outcrop.

5. DISCUSSION

5.1 Current Activity during Siltstone Deposition

Differences between settling velocity distributions of light and heavy mineral grains (Fig. 6) suggest that grain populations were sorted by two distinct processes. In all samples, heavy mineral and light mineral grains in the fine fraction (smaller than their respective population means) have nearly identical terminal fall velocity distributions, i.e. they are hydraulically equivalent. This suggests that the fine fraction was sorted primarily by settling. In contrast, the coarse fraction of light mineral grains is better sorted than the coarse fraction of heavy mineral grains and the fine fractions of both populations: there are fewer large light mineral grains than would be predicted by hydraulic equivalence with heavy mineral grains or by the distribution of fine light mineral grains. Moreover, heavy and light mineral grains having sizes greater than about 1.0–1.5 standard deviations above their respective population means have nearly *size-equivalent* distributions. This suggests that the coarse fraction has been additionally sorted by mobilization of large protruding grains, almost independently of density. The most likely sorting mechanism was rolling of exposed grains by weak currents over the relatively flat surfaces formed by beds of more abundant average-diameter particles. Heavy mineral grains were effectively shielded by larger light mineral grains (Slingerland and Smith, 1986).

Grain orientations in the black and brown siltstone facies are consistent with weak reworking currents that mobilized grains by rolling. Grains in both facies have bimodal distributions of inclinations nearly symmetric about 0° (flat-lying) along the channel axis, dipping with and against flow indicators in overlying sandstones. This is a stable orientation for elongate grains on a bed surface composed of similarly sized grains, and reflects a lack of currents flowing along the channel axis. Samples cut perpendicular to the channel axis exhibit unimodal, asymmetric dip distributions, likely reflecting reworking by weak currents flowing across the channel.

A maximum velocity for these reworking currents can be estimated based on the observation that modal grains in the black and brown siltstones were not mobilized. Using the incipient shear velocity for coarse silt, a flow depth of 10 m in the center of the channel, and a bed roughness coefficient of .41, the law of the wall predicts a maximum velocity of 24 cm/s across the top of the channel. This velocity and flow azimuth is consistent with a contour current, which are generally 5–30 cm/s (Hollister, 1993). Notably, grains of the average size observed in these facies settling through 10 m (the maximum observed compacted channel thickness) in a cross current of 24 cm/s would drift by ~1.2 km, which is greater than the width of the channel. Thus, the same current that reworked the black siltstone would have limited deposition of silts in the channel axis, consistent with the observed distribution of this facies.

Despite preserving evidence of reworking by weak contour currents, the study location lacks any evidence of the passage of turbidity currents immediately following channel formation. The first clear evidence of such currents comes in lags embedded in brown siltstones recording bypass of high-energy channel-confined turbidity currents. The localization of the brown siltstone to discontinuous bodies in the channel center suggests that both silts and lag sands were transported and deposited by turbidity currents.

5.2 Siltstone Diagenesis

Diagenetic carbonate precipitation is promoted by processes occurring in the anaerobic zones of sediments (Visscher et al., 2000), and prior studies of the Brushy, Bell and Cherry Canyon Formations have suggested that organic-rich sediments were carbonate cemented, perhaps prior to burial (Hays et al., 1996; Tice et al., submitted). Consistent with these suggestions, black siltstones in the study area contain substantially more carbonate cement than brown siltstones, suggesting cementation prior to compaction. Contacts between these two facies are sharp, as is the change in calcite content (Fig. 8c). This also suggests that the black siltstone was cemented prior to the deposition of the

brown siltstone as there was no likely permeability contrast that would have inhibited fluid flow or cementation in the brown siltstone. Finally, black siltstone clasts in overlying sandstone beds show that the primary silty sediment was cohesive or lithified prior to passage of turbidity currents despite the paucity of clay minerals. This also suggests early carbonate cementation.

It is likely that barite was also concentrated in the anaerobic zone of the black and brown siltstones. Marine organisms can contain three to four orders of magnitude greater Ba concentrations than seawater (Dean and Schreiber, 1978), and barite production in the modern ocean is associated with sinking and decaying organic matter (Ganeshram et al., 2003). Within sediments, microbial sulfate reduction depletes sulfate in pore fluids, remobilizing primary barite and producing Ba^{2+} -enriched fluids. When this fluid meets overlying sulfate-rich fluids at the top of the sulfate reducing zone, barite can reprecipitate as nodules or along laminations (Br  h  ret and Brumsack, 2000). Barite nodules are absent in organic-rich layers of the thinly bedded sandstone and structureless sandstone facies. This suggests that the accumulation of barite in discrete nodules in the black siltstone required that the sulfate reducing zone be fixed at a constant depth for a significant interval of time as during condensation (Br  h  ret and Brumsack, 2000; Torres et al., 1996).

5.3 Model for Channel Evolution

The lack of scouring along channel bases and irregular bed geometry has led investigators to interpret the slope channels at Salt Flat Bench as slump scars (Beaubouef et al., 1999; Gardner and Borer, 2000; Sageman et al., 1998). Subsequent deposition of a condensed section of black siltstone, most likely during a sea level highstand, is consistent with conditions likely to initiate slumping (Jacobi and Mitchell, 2002; Ross et al., 1994), i.e. rapid transgression. Slumping likely occurred in response to a rapid rise in relative sea level. In general, if the rate of sea-level rise exceeds sediment supply, sediments become trapped on the proximal ramp while the basin is starved. This leads

to progressive oversteepening of the upper slope resulting in slope failure, mass wasting, and slumping (Fischer and Sarnthein, 1988; Ross et al., 1994). The laminated siltstones incised by the channel at Salt Flat Bench appear darker and possibly more organic rich toward the base of the depression, suggesting decreasing deposition rates prior to slumping. This change is characteristic of marine transgression (Sageman et al., 1998). The period of maximum condensation occurs at the time of maximum sea level, after slope failure (Loutit et al., 1988; Ross et al., 1994).

During condensation, diagenesis of the draping carbonaceous siltstones resulted in their lithification while still at the sediment surface, possibly due to processes occurring in the anaerobic zone. Early cementation of this channel-lining facies may have stabilized upper ramp channels and limited the role of erosion by turbidity currents in shaping channel geometries and paths.

With the onset of forced regression, accommodation decreased and sediments were no longer trapped on the proximal slope (Ross et al., 1994). Sediment influx by turbidity currents increased as the source of sediments became closer to the basin. Continuing supply of coarse-grained clastic material led to channel filling and backfilling during the lowstand system tract (Gardner and Borer, 2000). A summary of channel initiation and evolution is presented in figure 10.

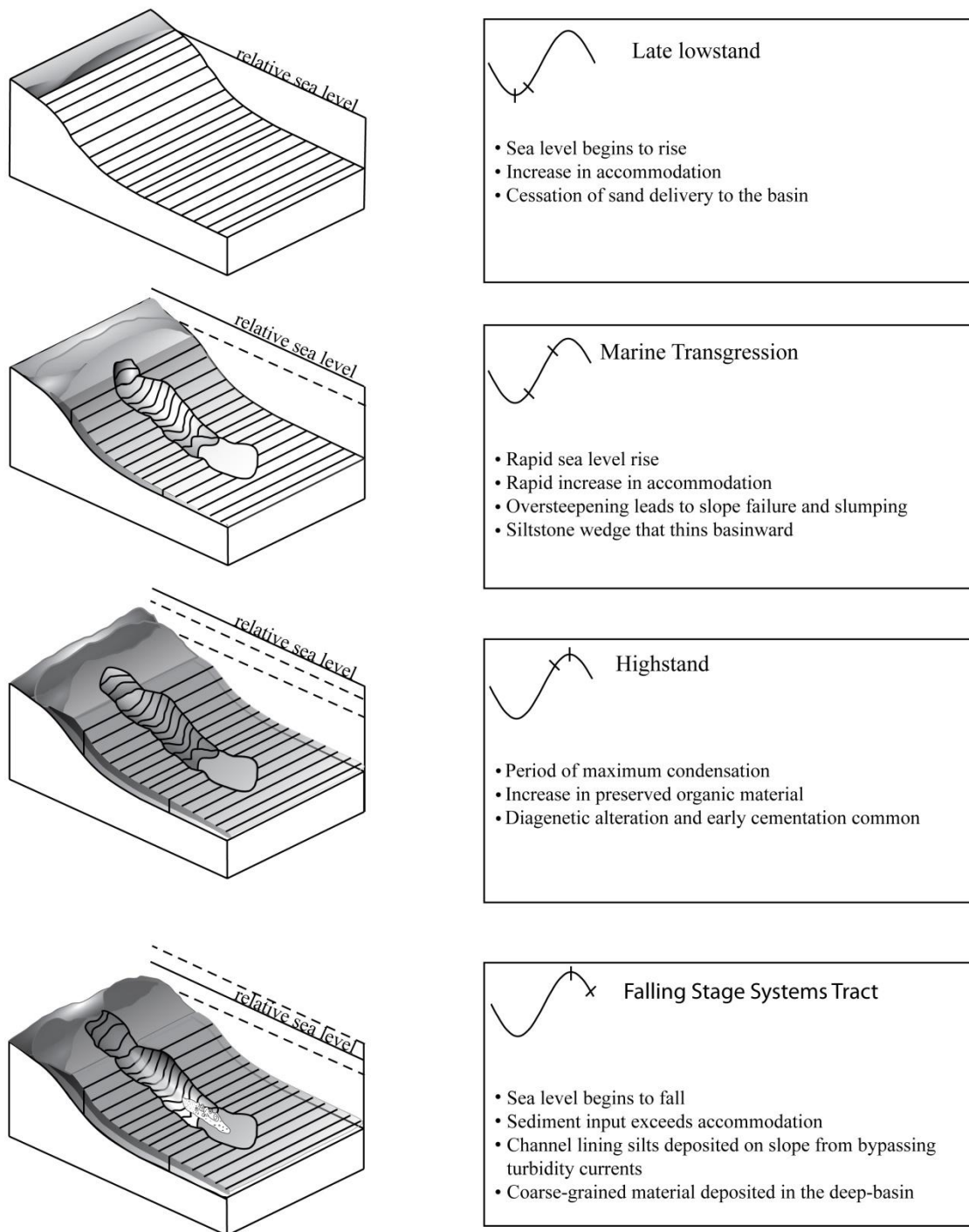


Figure 10: Model for channel initiation and early evolution at Salt Flat Bench.

6. CONCLUSIONS

This study identified three different facies of fine-grained sediments lining the paleo-channel exposed in the Salt Flat Bench: 1) a basal black siltstone deposited during condensation following slumping, 2) a lenticular brown siltstone deposited by primarily bypassing turbidity currents following condensation, and 3) a channel-marginal thinly bedded sandstone deposited by low density turbidity currents during channel backfilling. The relationship of these facies to the basal master surface suggests that turbidity currents were not flowing at significant volume immediately following slumping, and are unlikely to have contributed to erosion of the channel. The black siltstone is approximately four times thicker at the channel margin than at its axis, likely due to across-channel variations in deposition rates.

XRF microscopy allowed in situ visualization and measurement of heavy mineral populations at hand-sample scale for the first time. Heavy mineral and light mineral grain size distributions were consistent with experimental studies of grain shielding (Slingerland and Smith, 1986). Preferential grain orientations in both the black and brown siltstone facies are also consistent with the same reworking currents oriented perpendicular to the channel axis. The reorientation of these grains is most likely caused by contour currents just below the velocity required for incipient motion. The same currents were likely responsible for differential deposition rates of the black siltstone across the channel axis.

Authigenic barite and calcite formation in organic-rich layers of Brushy Canyon siltstones is consistent with the diagenesis in anaerobic sediments (Br  h  ret and Brumsack, 2000; Tice et al., 2011). Organically driven diagenesis played a significant role in channel formation by creating a bed surface resistant to erosion. Solidification of the black siltstone facies with calcite cement created a semi-permanent conduit for submarine density currents.

Most models for channel inception begin with turbidity currents as an erosional or depositional mechanism. There is a lack of levee deposits observed in outcrops of the Brushy Canyon Formation. By conventional models this leaves erosion as the mechanism for channel initiation (Imran et al., 2002). Maximum erosive power is expected during early lowstand (Beaubouef et al., 1999). This is inconsistent with field observations; channel initiation at Salt Flat Bench occurred during a period of condensation. This was followed by an interval dominated by sediment bypass as sea level began to fall. This model helps to explain the distribution of upper-ramp channels in the Brushy Canyon Formation which are strongly tied to the locations of up-dip feeder canyons; channel initiation in this environment was largely the product of mechanisms unrelated to erosive turbidity currents. Instead, channel migration during later intervals of active sediment transport by turbidity currents was constrained by old slump depressions that were stabilized by early diagenesis of condensed facies.

Outcrops of the Brushy Canyon Formation are used as analogues for the subsurface geology of the Brushy, Bell and Cherry Canyon Formations. As of the year 2000, these three formations cumulatively produced 351.9 MMbbl of oil (Dutton et al., 2003). With renewed interest in Permian Basin exploration, sequence stratigraphic models can reduce risk in petroleum exploration. Recognizing condensed sections and bypass surfaces is important for the development of sequence stratigraphic models (Carvajal and Steel, 2009). This distinction allows more accurate inferences of the location of coeval sediments in the context of a relative sea level curve. Improved understanding of the processes leading to channelization can lead to better models of subsurface channel geometries and distributions.

REFERENCES

- Beaubouef, R.T., Rossen, C., Zelt, F.B., Sullivan, M.D., Mohrig, D.C., et al., 1999. Field guide for AAPG hedberg field research conference: deep-water sandstones, Brushy Canyon Formation, west Texas. AAPG, Tulsa, Oklahoma.
- Bréhéret, J.G., Brumsack, H.J., 2000. Barite concretions as evidence of pauses in sedimentation in the Marnes Bleues Formation of the Vocontian Basin (SE France). *Sedimentary Geology*, 130(3-4): 205-228.
- Carvajal, C., Steel, R., 2009. Shelf edge architecture and bypass of sand to deep water: influence of shelf-edge processes, sea level, and sediment supply. *Journal of Sedimentary Research*, 79(9): 652-672.
- Dean, W.E., Schreiber, B.C., 1978. Authigenic Barite, Leg 41 Deep Sea Drilling Project. *Initial Reports of the Deep Sea Drilling Project*, 41: 915-931.
- Dutton, S.P., Kim, E.M., Broadhead, R.F., Breton, C.L., Raatz, W.D., et al., 2003. Play analysis and digital portfolio of major oil reservoirs in the Permian Basin: application and transfer of advanced geological and engineering technologies for incremental production opportunities. Bureau of Economic Geology, OSTI ID: 825581: 1-74.
- Fedele, J.J., García, M.H., 2009. Laboratory experiments on the formation of subaqueous depositional gullies by turbidity currents. *Marine Geology*, 258(1-4): 48-59.
- Filliben, J.J., 2010. *Engineering Statistics Handbook*. NIST/SEMATECH.

- Fischer, A.G., Sarnthein, M., 1988. Airborne silts and dune-derived sands in the Permian of the Delaware Basin. *Journal of Sedimentary Research*, 58(4): 637-643.
- Ganeshram, R.S., Francois, R., Commeau, J., Brown-Leger, S.L., 2003. An experimental investigation of barite formation in seawater. *Geochimica et Cosmochimica Acta*, 67(14): 2599.
- Gardner, M., 2003. Stratigraphic process-response model for submarine channels and related features from studies of Permian Brushy Canyon outcrops, west Texas. *Marine and Petroleum Geology*, 21(6): 779-781.
- Gardner, M., Borer, J., 2000. Submarine channel architecture along a slope to basin profile, Brushy Canyon Formation, west Texas, In: Mouma, A.H., Stone, C.G., (Eds.), *Fine-Grained Turbidite Systems*. AAPG Memoir, 72 (SEPM Special Publications 68): 195-214.
- Gardner, M., Borer, J.M., Melick, J.J., Kling, E.R., Baptista, N., et al., 2010. Evaluating source to sink controls on the Permian record of deep-water sedimentation in the Delaware Basin, west Texas, USA. *Search and Discovery* (#50247).
- Google, 2011. Topographic map of Guadalupe Mountains National Park. Google, Inc., Mountain View, CA. [http://maps.google.com/maps?q=topographic+map+guadalupe+mts+national+park&oe=utf-8&rls=org.mozilla:en-US:official&client=firefox-a&um=1&ie=UTF-8&hq=&hnear=Guadalupe+Mountains+National+ park,+Van+Horn+Rural,+TX&gl=us&t=p&ei=TzCvTfitG5Cy0QGw0f3ECw&sa=X&oi=geocode_result&ct=title&resnum=1&ved=0CCoQ8gEwAA](http://maps.google.com/maps?q=topographic+map+guadalupe+mts+national+park&oe=utf-8&rls=org.mozilla:en-US:official&client=firefox-a&um=1&ie=UTF-8&hq=&hnear=Guadalupe+Mountains+National+park,+Van+Horn+Rural,+TX&gl=us&t=p&ei=TzCvTfitG5Cy0QGw0f3ECw&sa=X&oi=geocode_result&ct=title&resnum=1&ved=0CCoQ8gEwAA), accessed 2/12/2011.

- Hardage, B.A., J. L. Simmons, J., Pendleton, V.M., Stubbs, B.A., Uszynski, B.J., 1998. 3-D seismic imaging and interpretation of Brushy Canyon slope and basin thin-bed reservoirs, northwest Delaware Basin. *Geophysics*, 63(5): 1507-1519.
- Harms, J.C., Brady, M.J., 1996. Deposition of the Brushy Canyon Formation: 30 years of conflicting hypothesis. In: W.D. Demis, A.G. Cole (Eds.), *The Brushy Canyon Play in Outcrop and Subsurface*. Permian Basin Section- Society of Economic Paleontologists and Mineralogists, pp. 51-61.
- Hays, P.D., Walling, S.D., Tieh, T.T., 1996. Organic and authigenic mineral geochemistry of the Permian Delaware Mountain Group, west Texas: implications for the chemical evolution of pore fluids. In: *Siliciclastic Diagenesis and Fluid Flow*. SEPM (Society for Sedimentary Geology), Tulsa, pp. 163-186.
- Imran, J.P., Parker, G., Harff, P., 2002. Experiments on incipient channelization of submarine fans. *Journal of Hydraulic Research*, 40: 21-32.
- Jacobi, R.D., Mitchell, C.E., 2002. Geodynamical interpretation of a major unconformity in the Taconic Foredeep: slide scar or onlap unconformity? *Physics and Chemistry of the Earth, Parts A/B/C*, 27(1-3): 169-201.
- Johnson-Ibach, L.E., 1982. Relation between sedimentation rate and total organic carbon content in ancient marine sediments. *AAPG Bulletin*, 66: 170-188.
- Julien, P.Y., 1998. *Erosion and Sedimentation*. Cambridge University Press, Cambridge.
- King, P.B., 1948. *Geology of the Southern Guadalupe Mountains, Texas*. U.S. Geological Survey Professional Paper 215: 183.

- Loutit, T.S., Hardenbol, J., Vail, P.R., Baum, G.R., 1988. Condensed sections: the key to age-dating and correlation of continental margin sequences. In: C.K. Wilgus et al. (Eds.), *Sea Level Changes—An Integrated Approach*, SEPM (Society for Sedimentary Geology), Tulsa, pp. 183–213.
- Pyles, D.R., Jennette, D.C., Tomasso, M., Beaubouef, R.T., Rossen, C., 2010. Concepts learned from a 3D outcrop of a sinuous slope channel complex: Beacon Channel Complex, Brushy Canyon Formation, west Texas, U.S.A. *Journal of Sedimentary Research*, 80(1): 67-96.
- Ross, W.C., Halliwell, B.A., May, J.A., Watts, D.E., Syvitski, J.P.M., 1994. Slope readjustment: a new model for the development of submarine fans and aprons. *Geology*, 22(6): 511-514.
- Rowland, J.C., Hilley, G.E., Fildani, A., 2010. A test of initiation of submarine leveed channels by deposition alone. *Journal of Sedimentary Research*, 80(8): 710-727.
- Sageman, B.B., Gardner, M.H., Armentrout, J.M., Murphy, A.E., 1998. Stratigraphic hierarchy of organic carbon-rich siltstones in deep-water facies, Brushy Canyon Formation (Guadalupian) Delaware Basin, West Texas. *Geology*, 26: 451-454.
- Slingerland, R., Smith, N.D., 1986. Occurrence and formation of water-laid placers. *Annual Review of Earth and Planetary Sciences*, 14(1): 113-147.
- Tice, M.M., Olszewski, T., Pope, M., Motanated, K., Unpublished results. Microbially promoted cementation and inorganic carbon burial on a Middle Permian deepwater ramp.

- Torres, M.E., Brumsack, H.J., Bohrmann, G., Emeis, K.C., 1996. Barite fronts in continental margin sediments: a new look at barium remobilization in the zone of sulfate reduction and formation of heavy barites in diagenetic fronts. *Chemical Geology*, 127(1-3): 125-139.
- Visscher, P.T., Reid, R.P., Bebout, B.M., 2000. Microscale observations of sulfate reduction: Correlation of microbial activity with lithified micritic laminae in modern marine stromatolites. *Geology*, 28(10): 919-922.
- Ye, Q., Kerans, C., 1996. Reconstructing Permian eustacy from 2-D backstripping and its use in forward models. *SEPM Special Publication*, 96-38: 69-74.

APPENDIX

Table A1: 16 samples collected from Salt Flat Bench for study of condensed sections and sediment bypass. TS refers to vertical sections from the eastern outcrop and GSFB refers to vertical sections from the western outcrop. The three colors represent different trips in chronological order.

Sample	Facies	Outcrop	Vertical Section
TS2E	Black siltstone	Eastern	2
TS2-2	Brown siltstone	Eastern	2
TS2-F	Transition from black to brown siltstone	Eastern	2
GSFB3-4	Brown siltstone	Western	3
GTS1-1	Brown siltstone	Eastern	1
GTS3-1	Brown siltstone	Eastern	3
GTS3-2	Brown siltstone	Eastern	3
GSFB3-A	Brown siltstone	Western	3
GSFB3-B	Brown siltstone	Western	3
GSFB3-C	Transition from black to brown siltstone	Western	3
GSFB3-D	Brown siltstone	Western	3
GTS2-A	Transition from black to brown siltstone	Eastern	2
GTS2B	Brown siltstone	Eastern	2
GTS2.5-A	Transition from black to brown siltstone	Eastern	between 2 and 3
GTS2.75-A	Brown siltstone	Eastern	between 2 and 3
GTS3-A	Transition from black to brown siltstone	Eastern	3

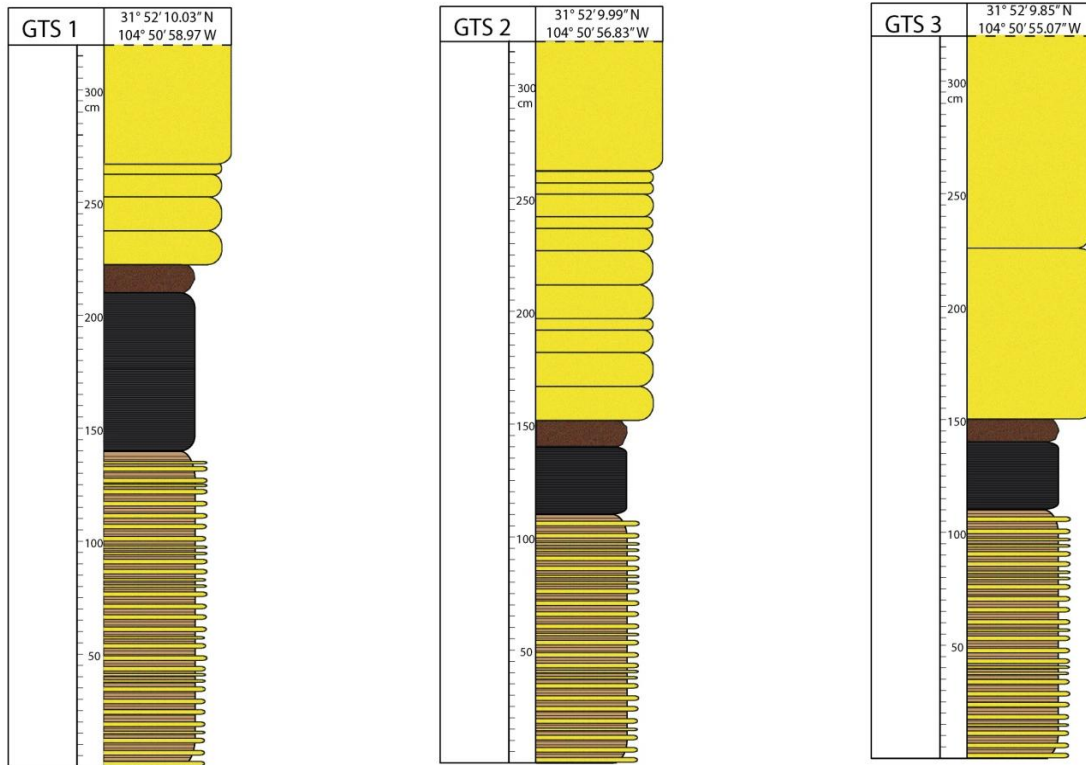


Figure A1: Vertical sections from the eastern outcrop.

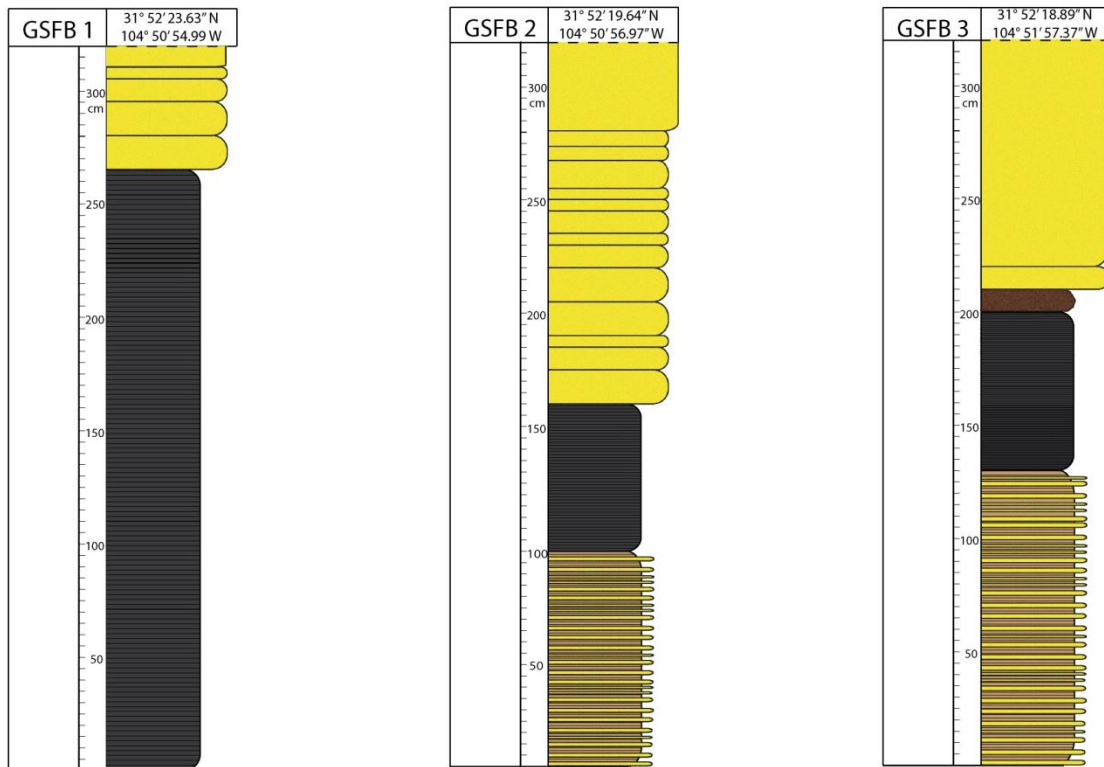


Figure A2: Vertical sections from the western outcrop.

VITA

Name: Spencer Blake Gunderson

Address: Department of Geology and Geophysics, MS 3115
Texas A&M University
College Station, Texas 77843-3115

Email Address: sbgunderson@gmail.com

Education: B.A., Geology, The University of California, Berkeley, 2008